Inner–outer interactions in rough-wall turbulence

D. T. Squire, W. J. Baars, N. Hutchins & I. Marusic

To cite this article: D. T. Squire, W. J. Baars, N. Hutchins & I. Marusic (2016): Inner–outer interactions in rough-wall turbulence, Journal of Turbulence, DOI: 10.1080/14685248.2016.1235278

To link to this article: http://dx.doi.org/10.1080/14685248.2016.1235278

JOURNAL OF TURBULENCE, 2016
http://dx.doi.org/10.1080/14685248.2016.1235278

Inner–outer interactions in rough-wall turbulence

D. T. Squire, W. J. Baars, N. Hutchins and I. Marusic

Department of Mechanical Engineering, University of Melbourne, Melbourne, Australia

ABSTRACT

Here we revisit the inner–outer interaction model (IOIM) of Marusic et al. (Science, vol. 329, 2010, pp. 193–196) that enables the prediction of statistics of the fluctuating streamwise velocity in the inner region of wall-bounded turbulent flows from a large-scale velocity signature measured in the outer region of the flow. The model is characterised by two empirically observed inner–outer interactions: superposition of energy from outer region large-scale motions; and amplitude modulation by these large-scale motions of a small-scale 'universal' signal (u^*), which in smooth-wall flows is Reynolds number invariant. In the present study, the inner–outer interactions in rough-wall turbulent boundary layers are examined within the framework of the IOIM. Simultaneous two-point hot-wire anemometry measurements enable quantification, via the model parameters, of the strengths of superposition and amplitude modulation effects in a rough-wall flow, and these are compared to a smooth-wall flow. It is shown that the present rough-wall significantly reduces the effects of superposition, while increasing the amplitude modulation effect. The former is true even in flows that exhibit outer region similarity. Using the model parameters obtained from the two-point measurements, predictions of inner region streamwise velocity statistics and spectra are compared to measurements over a range of friction and roughness Reynolds numbers. These results indicate that the u^* signal does depend on roughness Reynolds number (k_s^+), but is robust to changes in friction Reynolds number (δ^+). Additionally, the superposition strength is shown to be relatively independent of both roughness and friction Reynolds number. The implications of the present results on the suitability of the IOIM as a predictive tool in rough-wall turbulence are discussed.

ARTICLE HISTORY
Received 11 July 2016
Accepted 6 September 2016

KEYWORDS
Wall-bounded turbulence; rough walls; scale interaction

1. Introduction

In wall-bounded turbulence, the interactions between the near-wall and outer flow are of considerable interest. In addition to their obvious relevance to the dynamics and structure of the turbulence, these interactions govern the general response of wall-bounded flows to external influences on the near-wall region. Such influences include modifications to the wall-boundary condition, most commonly through the introduction of dynamically significant surface roughness. Examples of rough-wall bounded turbulence are commonplace across geophysical and engineering flows.

CONTACT D. T. Squire squired@unimelb.edu.au

The classical theory in rough-wall flows hypothesises that for *small* roughness at high Reynolds numbers, the outer region is wholly independent of the surface roughness, except through the influenced wall-layer height and wall stresses [1]. Here, *small* roughness implies a large difference between roughness scale(s) and wall-layer height, such that the outer region flow is sufficiently isolated from the direct influences of the roughness elements. In general, despite controversy in recent decades, the majority of existing evidence suggests that rough-wall flows which adhere to the above criteria exhibit approximate similarity in the outer region [2,3]. It is important to note here that there is a tendency in the literature to look for outer region similarity where it may not be expected. Certain roughness types with large wall-parallel length scales and/or high degrees of anisotropy can generate stationary features that penetrate deep into the wall layer (see, for example, [4–6]). Additionally, recent studies indicate that both the roughness and bulk Reynolds numbers must be high before similarity can be anticipated [3,7]. Nonetheless, the notion that outer region similarity can exist, even under specific circumstances, implies little consequence from modifications to the near-wall flow on outer layer dynamics, which may then question the importance of the wall in wall-bounded flows [8].

Following the observations of recurrent near-wall streaks by [9], many early studies have focused on investigating the near-wall region of smooth-wall flows. Certainly, interest in this region is justified by evidence that the small-scale streaks are associated with an autonomous and regenerative near-wall cycle [10,11], and that this cycle is responsible for the highest local levels of turbulence production across the wall layer. The relevance of this cycle at high Reynolds numbers, however, is difficult to predict. Indeed, as Reynolds number increases, the non-dimensionalised location and intensity of the near-wall cycle remains approximately fixed in viscous units, and the relative contribution to the bulk kinetic energy production from the outer layer increases. Thus, at sufficiently high Reynolds number, the logarithmic region becomes the major contributor to bulk production, with large-scale motions of $\mathcal{O}(\delta)$ playing a significant role [12]. (Marusic et al. [13] estimate that this occurs beyond friction Reynolds number, $\delta^+ \equiv \delta U_\tau/\nu \approx 4200$, where δ is the boundary layer thickness, U_τ is the wall friction velocity and ν is the kinematic viscosity.) Furthermore, there is considerable evidence in smooth-wall flows for interdependence between these large-scale motions and the small-scale turbulence throughout the entire wall layer [12,14,15]. In the near-wall region, the influence of the overlying large-scale motions on small-scale fluctuations can be aptly surmised as a combined effect of superposition and amplitude modulation [14,16]. Based on this observation, Marusic et al. [17] developed a predictive model to enable prediction of the near-wall streamwise velocity fluctuations from a large-scale velocity signal acquired in the outer region. Hereafter, this model is referred to as the inner–outer interaction model (IOIM).

The IOIM can be expressed as

$$u_p^+ = \underbrace{u_S^+}_{1} + \underbrace{u^* \left\{1 + \Gamma u_S^+\right\}}_{2}, \tag{1}$$

where u_p^+ is the predicted fluctuating streamwise velocity signal at z^+, obtained from the input velocity signal acquired within the logarithmic region. Here, the $+$ superscript denotes inner-normalised variables: length scales normalised by ν/U_τ; and velocity scales

normalised by U_τ. Term 1 in Equation (1) represents the superposed near-wall 'footprint' of the outer region large-scale fluctuations. The modulated small-scale signal is estimated by term 2, which describes modulation of the inner-scaled 'universal' signal, u^*, by these large scales. Here, the 'universal' signal represents the near-wall small-scale signal that would exist absent any large-scale influences (for a smooth wall, this is strongly tied to the near-wall cycle), and the coefficient Γ characterises the strength of the modulation effect. A calibration experiment involving two-point measurements of the streamwise velocity fluctuations is required to determine u^*, Γ, and the relation between the acquired large-scale signal and its superposed 'footprint', u_S^+. Details of this process are provided in [18,19], and in Section 3 of the present paper. It is worth noting here that accurate predictions of the near-wall streamwise turbulence intensity (and spectra) can be obtained using Equation (1) with $\Gamma = 0$. However, a non-zero Γ is necessary to predict odd-order moments of u_p^+. Additionally, application of the IOIM at Reynolds numbers distinct from that of the calibration experiment relies on the assumption that the 'universal' signal, u^*, is Reynolds number invariant. This assumption has been shown to be substantially valid in smooth-wall boundary layers, pipes and channels, such that accurate estimates of the inner layer spectra, moments up to the sixth order and fluctuating wall shear stress can be predicted from an outer layer input over a wide range of Reynolds numbers [18,20].

Rough-wall flows are characterised by near-wall dynamical influences that are often interpreted as roughness-induced disturbances to the near-wall cycle [21,22]. Previous studies have demonstrated that these near-wall influences can be broadband, and are a function of roughness Reynolds number and geometry [7,22]. This would suggest that u^* is unlikely to be universal in most rough-wall flows. There are, therefore, two interesting questions that arise from the previous paragraphs. First, in the context of the IOIM, how do the inner and outer regions of rough-wall turbulent wall layers interact, and how does this differ from smooth-wall flows? This is particularly interesting in rough-wall flows that exhibit outer region similarity, since in these cases the large-scale input signal is approximately the same for smooth- and rough-wall flows. Further, is the IOIM appropriate and useful in rough-wall flows, given that u^* is likely to be roughness dependent? These are questions that we aim to address in the present paper.

1.1. The present contribution

Here we compare smooth- and rough-wall boundary layer flows in the context of the IOIM. Two-point hot-wire anemometry calibration measurements are utilised for each wall condition to quantify the strengths of near-wall superposition and amplitude modulation of large-scale log-region-based structures (Section 3.2). The rough-wall measurements are obtained above a well-characterised sandpaper roughness, and demonstrate statistical and structural outer region similarity (see [7,23]). Based on the calibration measurements and utilising existing rough-wall data, IOIM predictions of the near-wall streamwise velocity spectra, turbulence intensity and skewness are here compared to measurements across a range of roughness and friction Reynolds numbers (Section 3.3). These comparisons suggest that the IOIM is appropriate in rough-wall flows when the roughness Reynolds numbers of the calibration and prediction are approximately matched. Finally, practical implications of the results are discussed (Section 4).

All measurements presented herein were obtained in the High Reynolds Number Boundary Layer Wind Tunnel at the University of Melbourne using hot-wire anemometry sensors with inner-normalised length, $l^+ < 25$. Except where explicitly stated, a floating element drag balance is used to determine U_τ directly (see [7,24] for details). Throughout this paper, x, y and z denote the streamwise, spanwise and wall-normal directions. Mean and fluctuating quantities are denoted using upper- and lower-case variables, respectively. For the smooth-wall measurements, $z = 0$ is the location of the wall. However, for all rough-wall measurements presented herein, $z = z' + \epsilon$, where $z' = 0$ is located at the crest of the roughness, and ϵ is the wall offset parameter, required to account for the fact that the roughness displaces the entire flow outwards. Here, $\epsilon = 0.902$ mm, with justification for this value provided in [7]. Note that the boundary layer thickness is here defined as the wall-normal location at which the mean streamwise velocity is 99% of the freestream velocity, U_∞.

2. Near-wall roughness influences

Before investigating details of the IOIM in rough-wall flows, we first briefly consider the influence of surface roughness on near-wall boundary layer dynamics. In this paper, the roughness 'strength' is quantified by the inner-normalised equivalent sand grain roughness, k_s^+, which has been computed to collapse fully rough profiles taken above the present rough surface onto Nikuradse's empirically determined fully rough asymptote for sand grain roughness (details in [7,25]). The approach is common in the literature, and attempts to enable comparison of fully rough flows above geometrically different roughnesses through their net effect on the drag. Flows are commonly considered to be fully rough for $k_s^+ \gtrsim 70$, although this bound is only approximate [3,26]. We note that the behaviours discussed in this section can be equally expressed as a function of any other equivalent measure of the roughness-influence on the viscous sub-layer. Common examples are the roughness function, ΔU^+ [22], and the modified roughness length, z_0^+ [27].

In Figure 1, the pre-multiplied kinetic energy production, z^+P^+, is presented for smooth- and rough-wall flows. Here, in zero-pressure-gradient flows, the production is the product of the Reynolds shear stress and mean shear,

$$P^+ = -\overline{uw}^+ \frac{dU^+}{dz^+}. \tag{2}$$

When plotted in the present semi-logarithmic form, equal areas indicate equal integral contributions to the total production. The filled symbols in Figure 1 show rough-wall data with k_s^+ ranging from 37 to 97, where darker shading indicates a higher value of k_s^+. Despite lacking rough-wall data very near to the wall, a clear trend is apparent in Figure 1(a) for $z^+ \lesssim 200$, whereby the inner-normalised production is increasingly attenuated with k_s^+. These roughness-associated influences are apparently confined to the inner region of the boundary layer, resulting primarily from a reduction in the mean velocity gradient near the wall; beyond $z^+ \approx 200$, the smooth- and rough-wall production profiles show very similar behaviours. The smooth-wall profiles in Figure 1 demonstrate that with increasing Reynolds number, the location and intensity of the near-wall production peak remains approximately fixed in wall units, whereas the location of the outer peak apparently scales with δ (see Figure 1(b)). As a result, the logarithmic region, which lengthens in wall units

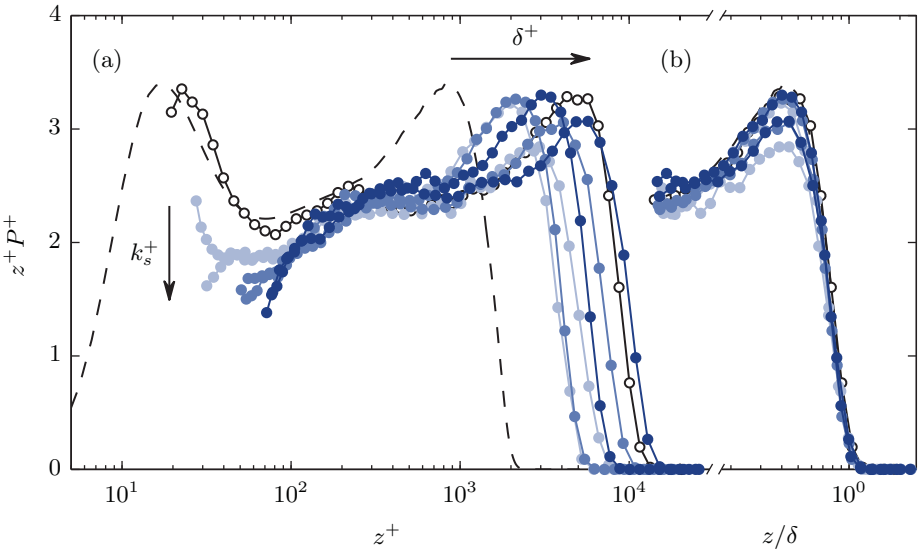

Figure 1. Pre-multiplied production, z^+P^+, in smooth- and rough-wall flows. Filled symbols show rough wall hot-wire data from [28], with darker shading indicating a higher value of k_s^+ (ranging from $k_s^+ = 37$ to $k_s^+ = 97$). Open symbols show smooth-wall hot-wire data from [29] (U_τ determined using the composite fit of [30]). The dashed black line shows smooth wall DNS at $\delta^+ \approx 2000$ [31].

with δ^+, contributes an increasing proportion of the total production as Reynolds number increases. This observation has been used in previous work to emphasise the importance of the logarithmic region at high Reynolds numbers [13,32]. Given the roughness-associated reduction in the near-wall production peak noted above, the argument for the importance of the logarithmic region appears to be even more relevant in rough-wall flows, especially for high k_s^+ (or equivalent).

The near-wall influence of the present rough surface is further scrutinised in Figure 2, which shows smooth- and rough-wall inner-normalised pre-multiplied energy spectrograms of the streamwise velocity fluctuations at $\delta^+ \approx$11,500 (Figure 2(a,c)). Also shown are the corresponding mean velocity and streamwise turbulence intensity profiles (Figure 2(b,d)). Two distinct high-energy sites are highlighted in the smooth-wall spectrogram. Near to the wall ($z^+ \approx 15$) a clear peak in the pre-multiplied spectra occurs at a length-scale close to $\lambda_x^+ \approx 1000$. This peak is due to the viscous-scaled elongated high- and low-speed regions associated with the near-wall cycle [9]. Additionally, at a location roughly centred on the logarithmic region, an outer peak is observed at length-scales that are many times larger than the boundary layer thickness ($\lambda_x \approx 6\delta$). The outer peak is associated with superstructures [12,16]; the energetic signature due to very elongated high- and low-speed events that have been observed to populate the logarithmic region of smooth-wall boundary layers, pipes and channels (see, for example, [33]). A similar outer energy peak is also observed at the same approximate location and scale in the rough-wall spectra in Figure 2(c). In fact, the distribution and magnitude of streamwise energy beyond $z/\delta \approx 0.06$ is very similar between the two wall conditions (the grey symbols in Figure 2(d) show the smooth-wall variance profile from Figure 2(b)). Squire et al. [23] also demonstrated for the

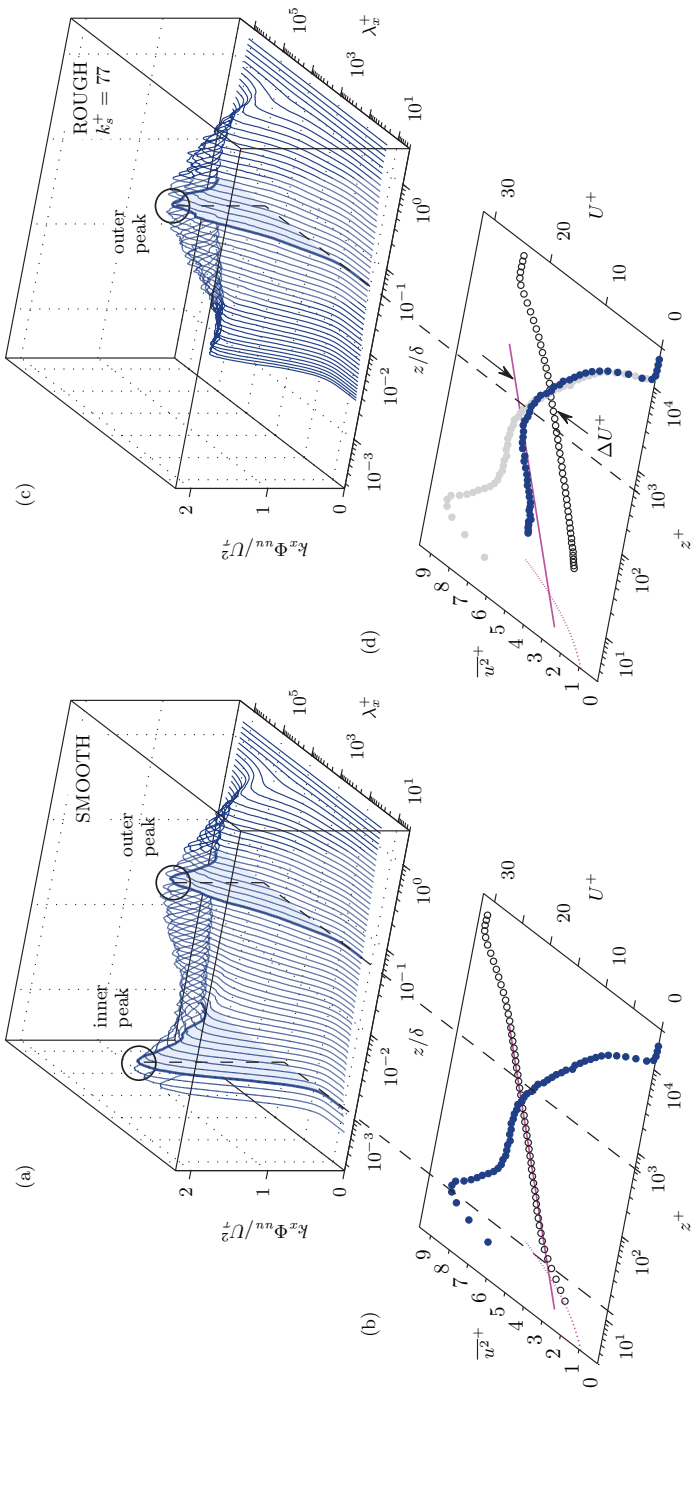

Figure 2. Pre-multiplied energy spectrograms of the streamwise velocity fluctuations in smooth-wall flows (a) and in rough-wall flows at $k_s^+ = 77$ (c). Smooth- and rough-wall data are from [34] (U_τ determined using the composite fit of [30]) and [7], respectively. For both cases, $\delta^+ \approx 11{,}500$. In (b) and (d), the corresponding smooth- and rough-wall mean streamwise velocity profile (○) and streamwise turbulence intensity profile (●) are shown. The solid and dotted lines show the smooth-wall logarithmic law ($\kappa = 0.384$, $A = 4.17$) and $U^+ = z^+$, respectively. In (d), the grey symbols show the smooth-wall turbulence intensity from (b) to facilitate comparison to the rough-wall profile.

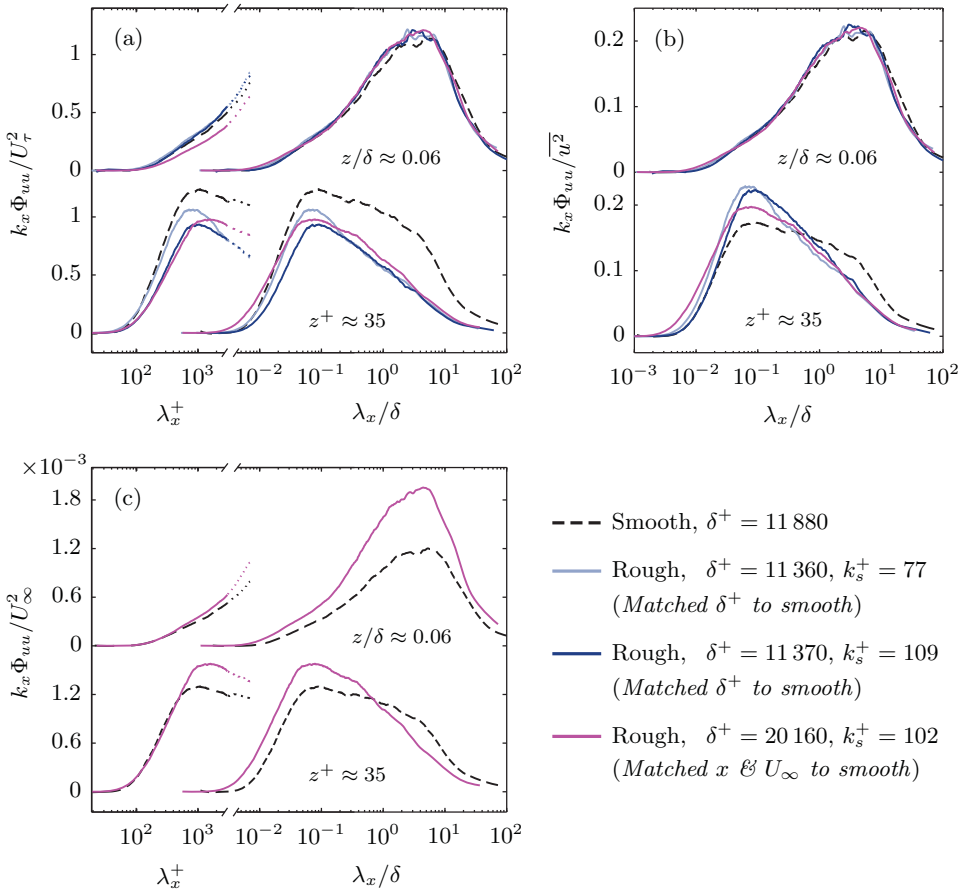

Figure 3. Comparison of smooth- and rough-wall pre-multiplied spectra of the streamwise velocity fluctuations. Smooth- and rough-wall data are from [34] (U_τ determined using the composite fit of [30]) and [7], respectively. The spectra are normalised by (a), U_τ^2; (b), $\overline{u^2}$; (c), U_∞^2. In each plot, spectral comparisons are presented at $z^+ \approx 35$ (bottom half of plot) and at $z/\delta \approx 0.06$ (top half of plot). Smooth-wall spectra are represented by dashed lines. Smooth- and rough-wall spectra are compared at matched δ^+ (see ——; ——) and for matched wind tunnel conditions (see ——) .

same rough-wall flow, outer region similarity of two-point correlations and spatial coherence of streamwise velocity fluctuations with those from smooth-wall flows at matched δ^+. Near to the wall, however, Figure 2(c,d) demonstrates that the inner-normalised rough-wall energy is significantly attenuated relative to the smooth-wall flow. The extent of near-wall attenuation has been shown to increase with k_s^+ [7,22]. This is demonstrated in the bottom half of Figure 3(a), which compares near-wall inner-normalised spectra from a smooth-wall flow (black dashed lines) with those from rough-wall flows at matched δ^+ but at two different values of k_s^+. (Note that the nearest wall-normal location at which the smooth- and rough-wall spectra can be compared is limited by the rough-wall measurements to $z^+ \approx 35$.) Recall also that a similar dependence on k_s^+ was observed near to the wall in the rough-wall production profiles in Figure 1(a).

Interestingly, the roughness-induced near-wall attenuation demonstrated in the bottom half of Figure 3(a) occurs across the majority of energy-containing scales. Additionally,

the degree of attenuation is scale dependent; this is demonstrated in Figure 3(b) where the same spectra are normalised by their respective integrated energy, $\overline{u^2}$. The energy in streamwise scales on the order of the roughness height, however, does not appear to be significantly influenced by the rough-wall (note that the present roughness height, $k \approx k_s/2$). Based on the near-wall flow visualisations of [21], previous studies have interpreted the roughness-associated reduction in near-wall inner-normalised streamwise turbulence intensity as evidence that the near-wall cycle has been influenced [7,22]. Certainly, the smooth-to-rough comparisons of Figures 1 and 3(a) indicate that, if such a cycle still exists in the present rough-wall flows, its contributions to the total production and streamwise turbulence intensity are apparently reduced by an amount that increases with k_s^+. However, this description is only appropriate for streamwise scales close to the smooth-wall inner energy peak ($\lambda_x^+ \approx 1000$), which, recall, is mostly produced by the near-wall cycle. In fact, the smooth- and rough-wall spectral comparisons in the bottom half of Figure 3(a) indicate that scales $\lambda_x^+ \gg 1000$ are responsible for the majority of the difference between the near-wall inner-normalised energy of the two flows. As was discussed in Section 1, the large-scale near-wall energy in smooth-wall flows is associated primarily with the superimposed 'footprint' of large-scale log-region-based energetic motions. Various assessments of the outer region flow above the present rough surface reveal similarity with smooth-wall flows over a range of δ^+ and (sufficiently high) k_s^+ (see [7,23] and the log-region spectral comparisons in the top half of Figure 3(a)). The implication then is that similar large-scale motions (in terms of inner-normalised energy and structure) inhabit the log-region of smooth- and rough-wall boundary layers, yet in the latter, the energetic 'footprint' of these motions on the wall is significantly reduced. This will be further investigated within the framework of the IOIM in Section 3.

A final interesting point arises from the spectral comparisons in Figure 3. In our discussions of Figure 3(a), we have referred repeatedly to near-wall 'attenuation' of inner-normalised rough-wall energy relative to smooth-wall flows. However, under matched physical conditions (i.e. x, U_∞, ν), one effect of roughening the wall is to significantly increase the wall-drag and hence wall friction velocity, U_τ. Therefore, normalisation by inner variables inhibits appreciation of the effect, in physical units, of introducing wall-roughness to a previously smooth-wall flow (for example, as occurs over time as the result of biofouling on the submerged surface of a ship [35]). In Figure 3, rough- and smooth-wall spectra obtained under matched physical conditions are also compared. These spectra, normalised by their associated freestream velocity, U_∞, are presented in Figure 3(c). Given that U_∞ is matched for each wall condition, these comparisons are representative of the relative dimensional energy content of each flow. The comparisons in Figure 3(c) show that the present rough wall significantly increases the intensity of streamwise velocity fluctuations in the outer layer, yet near to the wall, the total energy is similar for the two wall conditions. Additionally, when plotted as a function of λ_x^+, the near-wall spectra show intriguing collapse for scales $\lambda_x^+ \lesssim 1000$. Note that given the increase in U_τ associated with the rough wall, the collapse implies that in physical units, smaller energy containing scales are present in the rough wall than in the smooth wall. This observation brings about an interesting question regarding the appropriate scales in the near-wall region of rough-wall flows. Certainly, in smooth-wall flows, the near-wall cycle is an inner-scaled phenomenon, where the wall-drag, and hence U_τ, is comprised only of skin friction. In rough-wall flows, however, U_τ represents drag resulting both from skin friction and pressure forces at the wall,

and thus may not represent the appropriate velocity scale for such a cycle, if one indeed exists.

3. The inner–outer interaction model

In smooth-wall flows, the IOIM allows for accurate predictions of the streamwise velocity fluctuations in the inner region of wall-bounded flows. Only a single input from an outer position in the logarithmic region (i.e. the large-scale inner-normalised streamwise velocity) is required for predictions at any friction Reynolds number. All other intrinsic model parameters are determined from a once-off calibration experiment [18,19]. Application of the IOIM to a well-characterised rough-wall boundary layer flow aids in comprehending two aspects of rough-wall turbulence. First, we can glean a more elaborate understanding of the large-scale interactions between the near-wall and outer flow. This is motivated in part by the observation in the previous section that the near-wall 'footprint' of large-scale outer region structures differs for smooth- and rough-wall flows. Second, we may gain insight into the 'universality' of the turbulence in the inner region. Certainly, the results of the previous section indicate that the small-scale fluctuations in this region are at least a function of the roughness Reynolds number.

3.1. Description of the model

Following previous work in smooth-wall flows [16–19,36], the mathematical expression for the IOIM given in Equation (1) can be expressed in full as

$$u_p^+\left(z^+,t^+\right) = u^*\left(z^+,t^+\right)\left\{1+\Gamma\left(z^+\right)u_S^+\left(z^+,t^+\right)\right\} + u_S^+\left(z^+,t^+\right), \tag{3}$$

where u_S^+ is constructed via a spectral linear stochastic estimation, according to

$$\begin{aligned} u_S^+\left(z^+,t^+\right) &= \mathcal{F}^{-1}\left\{U_S\left(z^+;\,f^+\right)\right\} \\ &= \mathcal{F}^{-1}\left\{\widetilde{H}_L\left(z^+;\,f^+\right)\mathcal{F}\left[u_O^+\left(z_O^+,t^+\right)\right]\right\}. \end{aligned} \tag{4}$$

In Equations (3) and (4), $u^*(z^+,t^+)$, $\Gamma(z^+)$ and $\widetilde{H}_L(z^+;\,f^+)$ represent the calibration parameters of the IOIM. From a user's perspective, these parameters are known and can be derived from a two-point calibration experiment [19]. Therefore, the only required input to the IOIM is the time series $u_O^+(z_O^+,t^+)$, which represents the outer region velocity signal. From Equation (3), it is apparent that each predicted time series, $u_p^+(z^+,t^+)$, is constructed from two additive contributions: a large-scale superposition signature, u_S^+ (where subscript S denotes 'superposition'), and an amplitude-modulated, small-scale universal signal, $u^*(1+\Gamma u_S^+)$. Note that u^* is also inner-scaled with U_τ, but superscript + is omitted. Additionally, consistent with previous work, we refer to u^* as *the universal signal* throughout the following sections. As has been previously discussed, however, u^* is unlikely to be universal in most rough-wall flows.

The superposition component, u_S^+, consists of the perceived signature at prediction location z^+ that is linearly coherent with the input position, z_O^+. That is, u_S^+ is directly induced by the larger scale turbulence captured by the model's input, u_O^+. Baars et al. [19] recently adopted a linear stochastic estimation procedure to efficiently forge u_S^+ in the spectral

Table 1. Summary of the two-point hot-wire data acquired above the smooth and rough walls in the Melbourne wind tunnel.

Wall	δ^+	k_s^+	x (m)	U_∞ (m/s)	δ (mm)	U_τ (m/s)	l^+	z_O^+	z^+	Reference
Smooth	11,400	–	21	20.4	275	0.651	21	469	[11, 379][a]	[19]
Rough	14,700	77	21	15.0	367	0.600	20	546	[26, 402][b]	Present study

[a]Range spanned by 24 logarithmically spaced points.
[b]Range spanned by 25 logarithmically spaced points.

domain. Following Equation (4), a single computation results in the spectral-domain estimate, $U_S = \widetilde{H}_L \mathcal{F}[u_O^+]$, and is subsequently inverse Fourier-transformed to obtain time trace u_S^+. Here, $\widetilde{H}_L$ is a scale-dependent complex-valued transfer kernel comprising a gain and phase [19], and $\mathcal{F}$ denotes the Fourier transform with respect to time. For each z^+, the multiplication of the spectral-domain input and the linear kernel accounts for two effects: not only is the coherent turbulence superimposed on the prediction with a scale-dependent gain, but an inherent phase modification also accounts for the physical shift that is characteristic of the inclined large-scale structures in high-Reynolds-number wall-turbulence [12]. Note that the streamwise locations corresponding to the input (u_O^+) and prediction (u_p^+) time series are the same.

In addition to the superposition effect of u_S^+ on the prediction, it also functions as the modulation envelop of the smaller scale universal signal, $u^*(z^+, t^+)$; the strength of modulation is dictated by coefficient $\Gamma(z^+)$, which is a single scalar coefficient for each z^+. Physically, the universal signal is envisioned as the inner-scaled velocity fluctuations that would exist in the absence of any of the larger scale dynamics that are predominantly present in the outer region where the input is recorded. Consequently, the turbulence content of u^* is stochastically *incoherent* with the outer region and, as such, is fused with the *coherent* superposition imprint during prediction. A two-point hot-wire experiment, with synchronised recordings of the streamwise velocity fluctuations at each z^+, and fixed outer region position $z_O^+ > z^+$, provides the data for model calibration. Detailed descriptions of the calibration procedure can be found elsewhere [18,19]. The approach is to reverse the descriptions above, such that $\widetilde{H}_L(z^+; f^+)$, $u^*(z^+, t^+)$ and $\Gamma(z^+)$ can be determined from simultaneous measurements of the velocity signals at fixed z_O^+ and at a range of z^+ locations.

3.2. Smooth- and rough-wall calibration parameters

Simultaneous two-point hot-wire anemometry measurements have been performed above the smooth- and rough-walls to enable quantification of the model parameters described in the previous section. These data were taken at nominally matched friction Reynolds number (smooth: $\delta^+ = 11{,}400$; rough: $\delta^+ = 14{,}700$). Details of each calibration measurement are provided in Table 1. Note that the small discrepancy in δ^+ between the smooth- and rough-wall measurements has little consequence on our current work, as it has been demonstrated in smooth-wall flows that the model calibration parameters, when inner-normalised, are invariant with δ^+ [19]. That is, the smooth-wall calibration parameters are equal to those that would have been obtained from a smooth-wall calibration experiment at exactly matched δ^+ to the rough-wall case.

Figure 4(a,d) shows the gain of the linear transfer kernel, $|\widetilde{H}_L(z^+; f^+)|$, for the smooth and rough walls, respectively. Note that the spectral scale is presented in terms of a

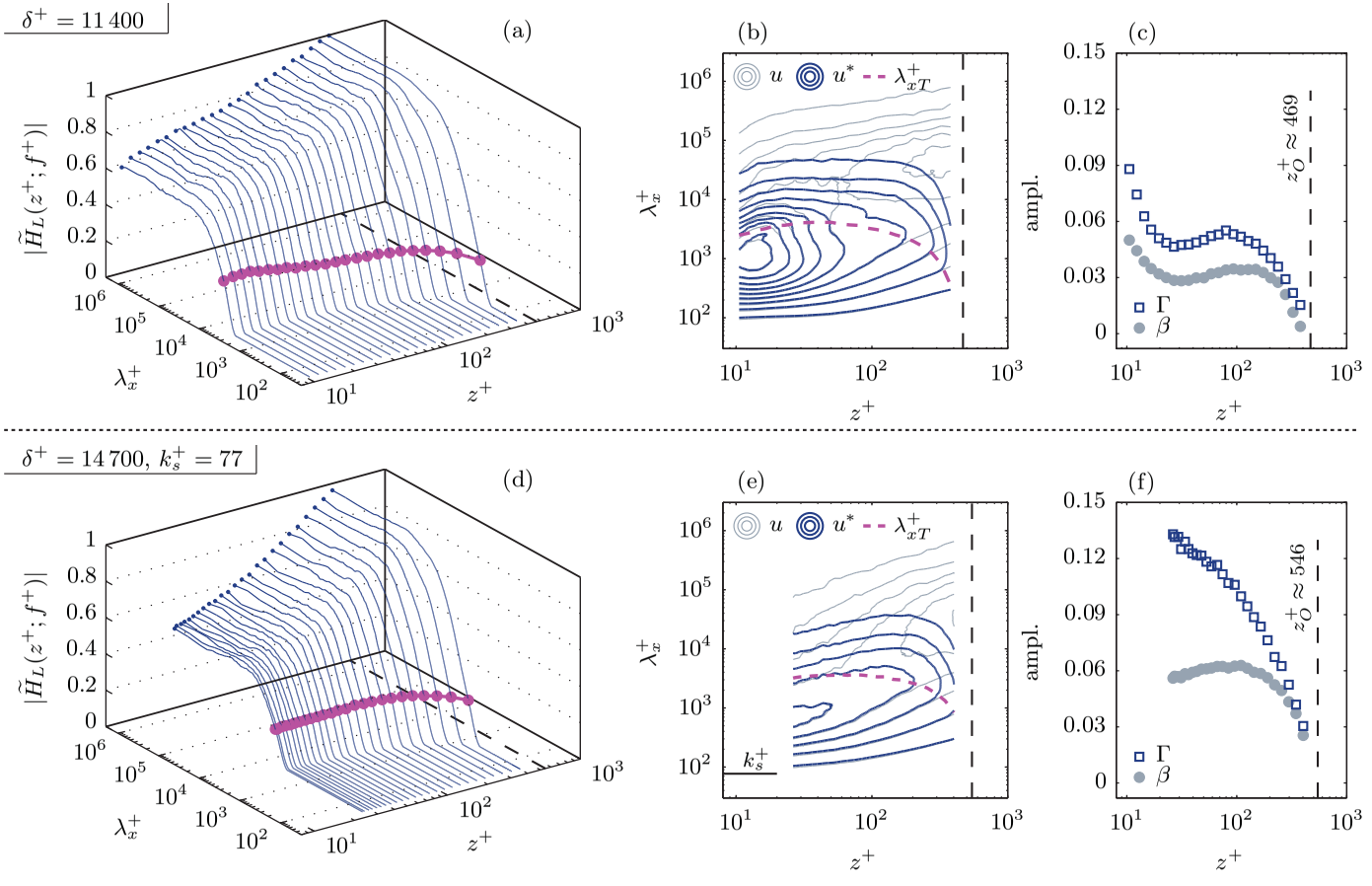

Figure 4. Model calibration parameters of the IOIM. (a) The gain of the linear kernel $\widetilde{H}_L(z^+; f^+)$ for every inner-scaled prediction location, z^+, derived from the smooth-wall calibration data. Joined dots show the coherence-threshold-based scale, λ_{xT}^+. (b) The pre-multiplied energy spectra of the streamwise velocity fluctuations of the universal signal, $k_x \Phi u^* u^* / U_\tau^2$ (___), and of the raw signal, $k_x \Phi uu / U_\tau^2$ (___). (c) Amplitude modulation coefficient, $\Gamma(z^+)$. (d–f) Similar to plots (a–c) but for the rough-wall calibration data. The position z_O^+ is indicated by a dashed black line in all plots.

spatial wavelength using Taylor's [37] frozen turbulence hypothesis and the local mean velocity. This approach has been shown to be substantially accurate for the streamwise velocity spectra in smooth- and rough-wall flows for $z^+ \gtrsim 100$ [38]. Note, however, that the outcomes of the present paper are unaffected by the accuracy of the spatial estimates. The positions of the fixed hot-wire in the outer region are $z_O^+ \approx 469$ and $z_O^+ \approx 546$ for the smooth and rough walls, respectively. These positions closely resemble the geometric centre of the log-region in each flow [7,39]. Previous smooth-wall studies have demonstrated that the deduced parameters of the IOIM are largely insensitive to changes in the location of the outer hot-wire probe, as long as this probe is located in the vicinity of the outer energy peak [36]. Given that outer region similarity is observed for the rough-wall calibration measurements, such that the inner-normalised outer energy site is apparently the same between smooth- and rough-wall flows, it is expected that the rough-wall calibration parameters are also insensitive to the location of the outer probe.

Regarding the smooth-wall kernel in Figure 4(a), the gain factor plateaus at the largest scales and exhibits a roll-off that occurs in the approximate range of $10^3 < \lambda_x^+ < 10^4$ (depending on wall-normal position). The roll-off is anticipated, given that small-scales are generally less spatially coherent. For reference, a wavelength λ_{xT}^+ at which the normalised coherence is less than 0.05 (for $\lambda_x^+ < \lambda_{xT}^+$) is indicated by the line connecting the individual kernels. At large λ_x^+, the plateau of $|\widetilde{H}_L|$ demonstrates that the large-scale content recorded in the outer region is superposed onto a near-wall position with a gain that is only weakly dependent on scale. For this range of scales, $|\widetilde{H}_L|$ is near unity for $z^+ \approx z_O^+$ and reduces to $\sim$0.6 for $z^+ \approx 10$. The decrease in gain factor towards the wall is a combined effect of a reduction in large-scale energy, relative to the outer region position, and a decrease in normalised coherence, which is unavoidable for increasing Δz, even for the largest wavelengths [19]. Comparing Figure 4(a) and (d), the general characteristics of the smooth-wall kernel remain present for the rough-wall flow. However, at all wall-normal locations, the plateau in $|\widetilde{H}_L|$ at large λ_x^+ is distinctly lower for the rough-wall case. For $z^+ < z_O^+$, the qualitative similarities between the smooth- and rough-wall kernels in Figure 4(a) and (d), respectively, provides evidence that the interaction, or linear coupling, between the inner and outer regions in these two flows are mechanistically comparable. That is to say, that apparently similar outer region structures superpose large-scale energy near to the wall in both the smooth- and rough-wall case (perhaps supporting a deeper reflection of Townsend's [1] wall-similarity hypothesis). However, as was demonstrated in Section 2, this effect is significantly weaker in rough-wall flows. At $z^+ = 35$, for example, the rough-wall plateau in $|\widetilde{H}_L|$ in Figure 4(d) is approximately 70% of that found for the smooth-wall at the same approximate location. Note that, while we have only considered the gain of $\widetilde{H}_L$ in Figure 4, the degree of physical (forward) inclination of the coherent large-scale structures is embedded in the phase of the complex kernel (see [19]). Squire et al. [23] have demonstrated that the inclination angle of these structures is similar between the present smooth- and rough-wall flows.

The pre-multiplied spectra of the smooth- and rough-wall universal signals, u^*, as determined from the two-point calibration data, are shown in Figure 4(b,e), for the smooth- and rough-wall, respectively. Spectrograms of the raw acquired signals are shown in the same plot to demonstrate the portion of the spectrogram considered by the IOIM to be universal (recall our previous warning about the use of the word 'universal' in the rough-wall case). Logically, for $\lambda_x^+ < \lambda_{xT}^+$, where there is an absence of any coherence between the boundary

layer content at z^+ and z_O^+, the majority of turbulent energy is captured by u^*. For $\lambda_x^+ > \lambda_{xT}^+$, the energy in u^* diminishes as these scales become coherent with those at z_O^+. These large scales are governed by superposition as described in the previous paragraph (see [18,19] for an elaborate discussion of the smooth-wall universal signal). Since the modulation parameter Γ does not noticeably affect the spectral content of u_p^+ (the modulation in Equation (4) is energetically weak and primarily affects odd-order moments), the model calibration may be interpreted as a spectral decomposition of the original content (i.e. u^+) into large-scale contributions that are coherent with u_O^+ (i.e. the spectrum of u_O^+ multiplied by $|\widetilde{H}_L|^2$), and small-scale contributions that are not (i.e. u^*). In this sense, the observation that u^* covers a similar range of λ_x^+ for the smooth and rough walls (i.e., λ_{xT}^+ is similar for both wall conditions) can be predicted from the qualitative similarities between the kernels in Figure 4(a,d). Despite exhibiting a similar range of energy containing scales, however, the inner-normalised energies of the smooth- and rough-wall universal signals are distinctly different. This result has implications on the practicality of the IOIM in rough-wall flows. Indeed, if the rough-wall universal signal depends strongly on the specific roughness and flow conditions (e.g. roughness morphology, k_s^+ and δ^+), then the use of the IOIM as a predictive tool in rough-wall flows is restricted. This is addressed further in Section 3.3.

The strength of amplitude modulation of u^* is compared for the smooth and rough walls in Figure 4(c) and (f), respectively. Two representations of the modulation strength are provided. Wall-normal profiles of $\Gamma(z^+)$ reflect the strength of modulation at each z^+ by the envelope given by $u_S^+(z^+, t^+)$ (see Equation 3), and thus the strength of modulation relative to the superposition of large-scale energy from the outer region. In addition, since the superposition signature has different amplitudes for the smooth- and rough-wall cases, we have also demonstrated the modulation relative to the large-scale signal in the outer region, represented by $\beta(z^+)$. This is included for consistency with previous work using the IOIM [18] using the same notation. Comparison of the smooth- and rough-wall modulation strengths in Figure 4(c,f) indicates that the modulation is significantly stronger in rough-wall flows. A similar observation has been made in rough-wall flows by [40,41]. This implies that the scale-interaction in rough-wall flows is stronger than in smooth-wall flows. In smooth-wall flows, modulation in the near-wall region can be posed as a consequence of large-scale variations in the wall-shear stress, τ_w [42–44]. These variations result from, and are proportional to, large-scale near-wall streamwise velocity fluctuations. That is, $\tau_w \propto u_S$ or $U_\tau \propto \sqrt{u_S}$, where recall u_S is the large-scale superposition signature. Large-scale variations in U_τ are observed as quasi-steady from the viewpoint of small-scale velocity fluctuations. Since the latter are believed to scale on viscous units (with a length scale and magnitude proportional to ν/U_τ and U_τ, respectively), their amplitude varies according to U_τ ($\propto \sqrt{u_S}$). In rough-wall flows, similar arguments can be made. However, here the near-wall flow also comprises small-scale turbulence associated with separation/shedding from the roughness elements (inducing pressure drag). Following simple dimensional arguments, one would expect the magnitude of these fluctuations to be proportional to the large-scale velocity fluctuations ($\propto u_S$). Thus, for rough-wall flows at high k_s^+ (i.e. where the pressure drag constitutes a large proportion of the total wall-drag), one might expect near-wall modulation to be stronger than in smooth-wall flows. Certainly, this description is consistent with the present findings, and with the near-wall modulation trends reported in existing rough-wall studies [40,41]. It is important to note here that these studies investigate scale interactions using the amplitude modulation coefficient: the normalised cross-correlation coefficient

between the near-wall large-scale velocity signal and an envelope of the small-scale fluctuations [36]. Under the framework posed above, this coefficient would also increase in rough-wall flows.

3.3. Rough-wall predictions

We turn our attention now to scrutinising the IOIM as a predictive tool in rough-wall flows. In this section, the rough-wall calibration parameters from the previous section are used to predict time-series of the streamwise velocity fluctuations in the inner region of rough-wall flows, and these predictions are compared to direct measurements. Such an approach has been successful in smooth-wall flows in predicting time-series that are statistically representative of the actual turbulence (spectral content and moments up to sixth order) over a wide Reynolds number range [18,19]. However, under zero-pressure gradient conditions, the smooth-wall turbulent state is completely governed by just one similarity parameter (δ^+). Therefore, given that the calibration experiment that is performed at sufficiently high δ^+ (such that an adequate scale-separation is guaranteed – see [12]), predictions can be made at any δ^+ using the set of Reynolds number invariant calibration parameters. In rough-wall flows, there is at least one additional relevant scale associated with the roughness geometry, making the application of calibration parameters in flows distinct from that of the calibration measurement less trivial. Here, we consider the extent to which changing δ^+ and k_s^+ affects the validity of rough-wall predictions made using the IOIM. For all predictions made below, single-component hot-wire anemometry data from [7] provide both the log-region input to the model, and the direct near-wall measurements against which the predictions are compared.

In Figure 5, measured and predicted near-wall streamwise velocity spectrograms, and profiles of turbulence intensity and skewness are compared at two friction Reynolds numbers distinct from that of the calibration measurement ($\delta^+ = 5250$ and 11,360 in the first and second columns, respectively). In both comparisons, k_s^+ is approximately matched to that of the calibration measurement, which, recall, was carried out at $\delta^+ = 14{,}700$ and $k_s^+ = 77$. In Figure 5, direct measurements are indicated by light markers, while predictions are overlaid using dark markers. The dashed line indicates the position of the input to the model. In general, excellent agreement is observed between the IOIM predictions and the direct measurements at both Reynolds numbers. In contrast, Figure 6 compares the measured and predicted near-wall streamwise fluctuations in rough-wall flows with k_s^+ distinct from that of the calibration measurement ($k_s^+ = 38$ and 109 in the first and second columns, respectively). Note that the friction Reynolds numbers in these comparisons are approximately matched to those in Figure 5. Assessments of the measured and predicted fluctuations in Figure 6 exhibit noticeably poorer agreement than in Figure 5. The differences are most apparent near to the wall, where a reduction in k_s^+, relative to the calibration measurement, generates increased and reduced streamwise turbulence intensity and skewness predictions, respectively (vice versa for increased k_s^+). It is evident from the spectrograms in Figure 6(b,d) that the discrepancies between predicted and measured turbulence intensities result, for the most part, from inapplicability of the universal signal in these flows. That is, the spectrograms show clear differences for $\lambda_x^+ < \lambda_{xT}^+$ that are consistent with the incorrect predictions of $\overline{u^2}^+$. This behaviour is unsurprising given that the flow close

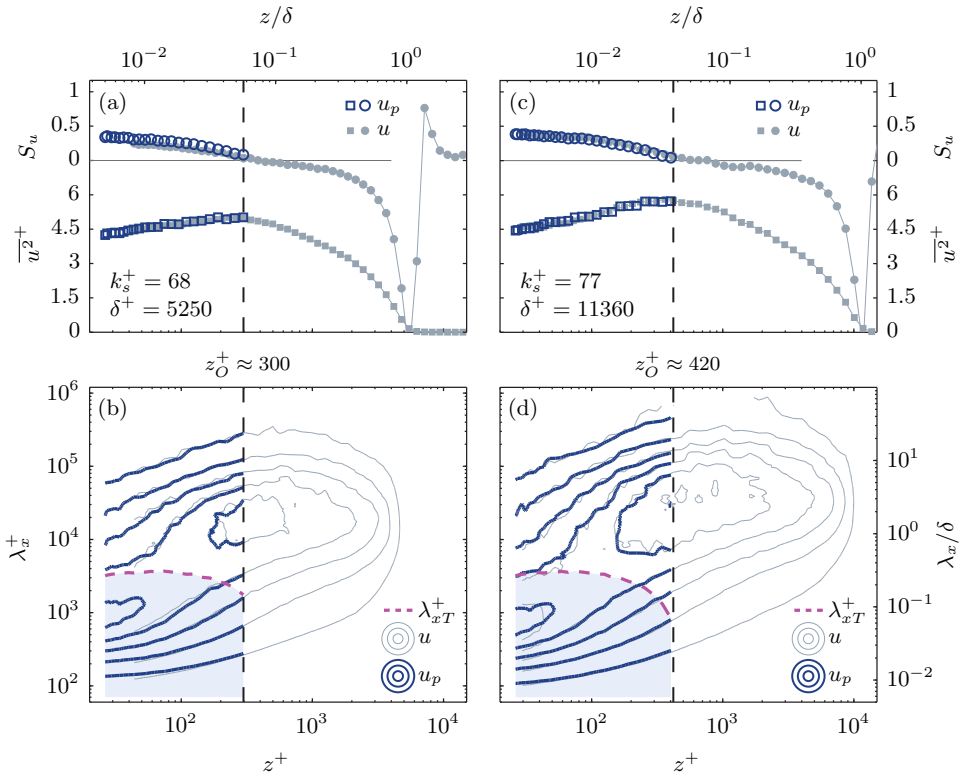

Figure 5. Predictions of rough-wall streamwise velocity fluctuations using the calibration parameters in Figure 4. The predictions are made using single-point HWA data with k_s^+ approximately close to that of the rough-wall calibration data, but at different friction Reynolds numbers [7]. (a) and (c) compare the predicted (empty symbols) and measured (filled symbols) turbulence intensity (squares) and skewness (circles) profiles. Similarly, (b) and (d) compare the predicted (——) and measured (——) pre-multiplied energy spectra. The position z_O^+ is indicated by a dashed black line in all plots.

to the roughness is characterised by motions whose size and energy are directly related to the roughness scale(s) [45]. Interestingly, however, despite these small-scale differences, the predicted and measured spectrograms still collapse reasonably well for $\lambda_x^+ > \lambda_{xT}^+$, indicating that the superposition component of the prediction is still valid, even when k_s^+ does not match the calibration data. This is also demonstrated in Figure 3(a), where changing k_s^+ at fixed δ^+ affects only the small-scale portion of the inner-normalised rough-wall spectra.

The results of Figures 5 and 6 propound some interesting characteristics of inner–outer interactions in rough-wall flows. The demonstrated agreement between model predictions and direct measurements in Figure 5 indicates that all calibration parameters of the IOIM, including u^*, are relatively robust to δ^+ when k_s^+ is approximately fixed. This observation has practical implications in developing boundary layers over rough surfaces where U_τ, and hence k_s^+, varies only slowly with downstream distance (see, for example, the developing rough-wall boundary layer measurements of [7]). Unfortunately, we lack rough-wall data to thoroughly test the observation at Reynolds numbers higher than that of the calibration measurement. This being said, in the bottom half of Figure 3(a), we compared near-wall inner-normalised streamwise velocity spectra in rough-wall flows at approximately

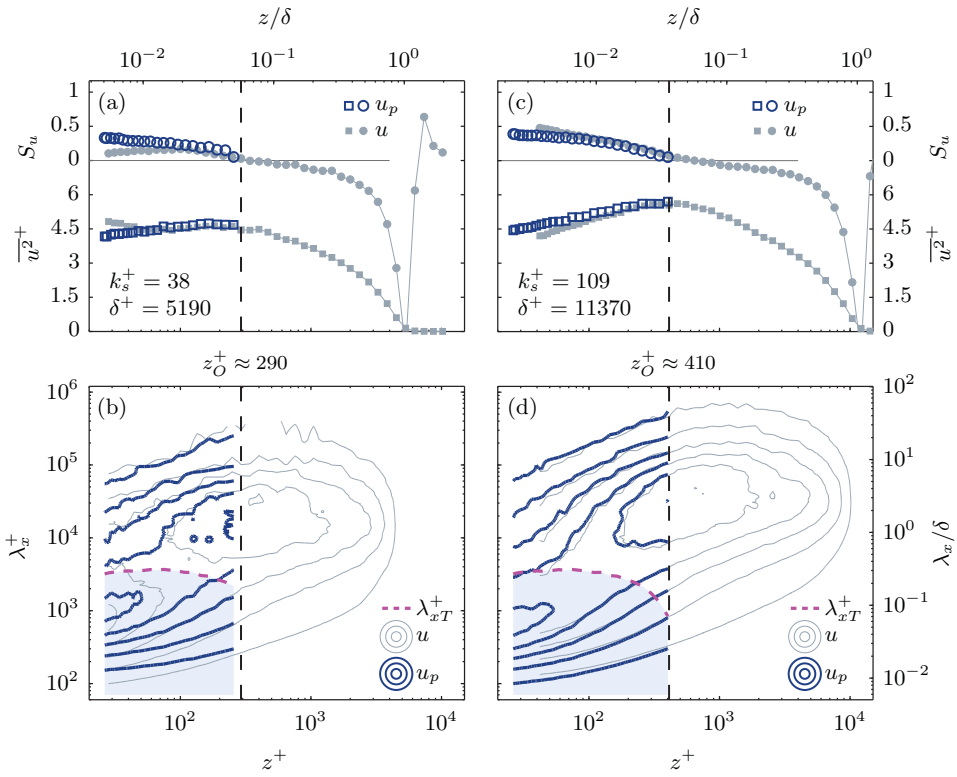

Figure 6. As in Figure 5, but here the predictions are made using single-point HWA data with k_s^+ distinct from that of the rough-wall calibration data. Note that the friction Reynolds numbers presented here approximately match those given in Figure 5.

matched k_s^+ ($k_s^+ \approx 100$) but with greatly different δ^+ ($\delta^+ = 11{,}370$ and $\delta^+ = 20{,}160$) – see the light blue and magenta lines in this figure. These spectra show reasonable collapse for scales $\lambda_x^+ \lesssim 1000$, indicating that their small-scale energy content, and hence perhaps their associated universal signals, are similar. Further measurements are required to consolidate this proposition. Figure 6 shows that in flows where k_s^+ does not approximately match that of the calibration measurement, the IOIM yields inaccurate predictions of the near-wall velocity fluctuations. However, even in these cases, the predicted large-scale near-wall energy content resulting from the superposition component of the IOIM ($\lambda_x^+ \gg \lambda_{xT}^+$) is still generally valid, indicating that the rough-wall linear transfer kernel (Section 3.2) is relatively independent of k_s^+. This is apparently true even at $k_s^+ = 38$, where outer region similarity is not observed (see the first column of Figure 6). It is important to note, however, that as $k_s^+ \to 0$, the rough-wall transfer kernel must approach that of the smooth wall. Regarding the discrepancies between predicted and measured skewness profiles in Figure 6, the IOIM predicted skewness arises from only two sources: skewness present in u^*, and/or skewness introduced by the modulation, the latter being a true scale interaction. Further studies, in which synchronised two-point calibration experiments are performed across a range of k_s^+, can determine whether the modulation coefficient is also a function of k_s^+.

We offer two cautionary statements pertaining to the results of this study. First, the rough-wall IOIM calibration measurements were obtained in the present study in a flow that was close to fully rough [7]. The observations discussed in the previous paragraph – in particular that accurate rough-wall IOIM predictions can be obtained for a range of δ^+ when k_s^+ is approximately matched to that of the calibration – may not necessarily be expected to hold when the calibration parameters are obtained deep in the transitionally rough regime. Second, all rough-wall measurements in the present study were performed above the same sand paper roughness. Certainly, the near-wall dynamics of rough-wall flows depend strongly on roughness morphology. We therefore caution the reader against assigning the results of the present study – particularly those relating to the universality of u^* – to flows above roughness morphologies significantly different than the present sand grain roughness.

4. Conclusion

The interactions between the inner and outer regions of rough-wall turbulent boundary layers have been examined within the framework of the IOIM [17]. Two empirically observed interactions are characterised by the model. Namely, a strong correlation between the large-scale energy in the inner and outer regions (superposition); and modulation of the intensity of the near-wall small-scale velocity fluctuations by large-scale outer region events (amplitude modulation). In the context of the IOIM, these small-scale velocity fluctuations are captured in a single term, u^*, which in smooth-wall flows is invariant with Reynolds number [18,19]. In the present rough-wall study, the IOIM has been employed as an analytical tool and assessed as a predictive tool. For the former, synchronised two-point hot-wire anemometry measurements have been used to compare, via the IOIM calibration parameters (namely, $\widetilde{H}_L$ and Γ), the strengths of superposition and amplitude modulation effects in a rough-wall flow ($\delta^+ = 14{,}700$, $k_s^+ = 77$) and smooth-wall flow ($\delta^+ = 11{,}400$). Using the rough-wall calibration parameters, predictions of inner layer streamwise velocity statistics and spectra are compared to direct measurements over a range of roughness Reynolds numbers ($38 < k_s^+ < 109$) and friction Reynolds numbers ($5190 < \delta^+ < 11{,}370$).

Ingeneral, the outcomes of this study can be summarised as follows:

(1) Compared to smooth-wall flows, the linear interaction between inner and outer region large-scale energy content is significantly weaker in rough-wall flows. Interestingly, the present results suggest that the shape and extent of the large-scale motions that contribute to this interaction are similar between the two flows (see the qualitative similarities between the smooth- and rough-wall transfer kernels in Figure 4(a,d)). However, near to the wall, the energy of these large-scale coherent events is lower in the rough-wall case. In addition to reduced superposition strength, the present rough wall also demonstrates a substantial increase in the strength of inner region amplitude modulation relative to the smooth-wall flow. Similar observations have been made in previous rough-wall studies [40,41]. Here we advocate that the increase in rough-wall modulation strength can be explained by considering the response of the small-scale turbulence to quasi-steady large-scale streamwise

velocity fluctuations. Where in smooth-wall flows it can be argued that the amplitude of small-scale fluctuations change proportionally to the *square root* of near-wall large-scale fluctuations, in rough-wall flows, the magnitude of small-scale turbulent motions associated with separation/shedding from the roughness elements is expected to be *linearly* proportional to large-scale fluctuations. Presumably, these roughness-induced motions contribute an increasing proportion of the total near-wall small-scale energy with increasing k_s^+.

(2) The IOIM can be used in rough-wall flows to make accurate predictions of inner region streamwise velocity statistics and spectra across a range of δ^+ when k_s^+ is approximately matched to that of the calibration measurement. The observation implies that the model calibration parameters, including u^*, do not depend strongly on δ^+. There is an important practical implication that arises here. In flows developing over unvarying rough surfaces, k_s^+ changes very slowly with streamwise position. Therefore, the present results indicate that predictions of the inner region development in such flows can be made from single large-scale outer region velocity measurements, and a calibration measurement (at the correct k_s^+), which can be performed at a low Reynolds number.

(3) The IOIM does not produce accurate predictions of inner region streamwise velocity statistics and spectra when k_s^+ is distinct from that of the calibration measurement. This being said, the large-scale linear transfer kernel, $\widetilde{H}_L$, is relatively insensitive to k_s^+. Thus, even where k_s^+ of the calibration and prediction are not similar, the large-scale portion ($\lambda_x^+ \gg \lambda_{xT}^+$) of the streamwise velocity spectra and associated statistics can be predicted. This is apparently true even for rough-wall flows that do not exhibit outer region similarity (see Figure 6(a,b)). Further synchronised two-point measurements are required to determine how the modulation strength, Γ, varies with k_s^+. It is worth noting, however, that if both $\widetilde{H}_L$ and Γ are robust to changes in δ^+ and k_s^+, then the statistics of the inner region of a given rough-wall flow may be characterised by the IOIM using a single-calibration measurement when u^* is known as a function of k_s^+. In smooth-wall flows, u^* follows the behaviour of a low Reynolds number flow, where the large-scale influences are weak [18]. Therefore, it is plausible that for a given rough-wall flow, $u^* = f(k_s^+)$ can be determined at low Reynolds numbers, for example, via direct numerical simulation. In this regard, it is particularly interesting to consider how/if u^* changes with k_s^+ for flows that are fully rough.

All current rough-wall measurements were obtained above the same sand grain surface. Further measurements above different surfaces are required to determine how the present results are affected by surface morphology.

Acknowledgments

This paper is dedicated to Professor Javier Jiménez on the occasion of his 70th birthday; his insights to turbulence and fluid mechanics in general are greatly valued.

Disclosure statement

No potential conflict of interest was reported by the authors.

Funding

The financial support was provided by Australian Research Council.

ORCID

D. T. Squire http://orcid.org/0000-0003-3271-6874
W. J. Baars http://orcid.org/0000-0003-1526-3084
N. Hutchins http://orcid.org/0000-0003-1599-002X
I. Marusic http://orcid.org/0000-0003-2700-8435

References

[1] Townsend AA. The structure of turbulent shear flow. Vol. 1. Cambridge (UK): Cambridge University Press; 1956.
[2] Flack KA, Schultz MP, Shapiro TA. Experimental support for Townsend's Reynolds number similarity hypothesis on rough walls. Phys Fluids. 2005;17:035102.
[3] Jiménez J. Turbulent flows over rough walls. Annu Rev Fluid Mech. 2004;36:173–196.
[4] Volino RJ, Schultz MP, Flack KA. Turbulence structure in boundary layers over periodic two- and three-dimensional roughness. J Fluid Mech. 2011;676:172–190.
[5] Nugroho B, Hutchins N, Monty JP. Large-scale spanwise periodicity in a turbulent boundary layer induced by highly ordered and directional surface roughness. Int J Heat Fluid Flow. 2013;41:90–102.
[6] Anderson W, Barros JM, Christensen KT, et al. Numerical and experimental study of mechanisms responsible for turbulent secondary flows in boundary layer flows over spanwise heterogeneous roughness. J Fluid Mech. 2015;768:316–347.
[7] Squire DT, Morrill-Winter C, Hutchins N, et al. Comparison of turbulent boundary layers over smooth and rough surfaces up to high Reynolds numbers. J Fluid Mech. 2016;795:210–240.
[8] Flores O, Jimenez J. Effect of wall-boundary disturbances on turbulent channel flows. J Fluid Mech. 2006;566:357–376.
[9] Kline SJ, Reynolds WC, Schraub FA, et al. The structure of turbulent boundary layers. J Fluid Mech. 1967;30:741–773.
[10] Jiménez J, Pinelli A. The autonomous cycle of near-wall turbulence. J Fluid Mech. 1999;389:335–359.
[11] Schoppa W, Hussain F. Coherent structure generation in near-wall turbulence. J Fluid Mech. 2002;453:57–108.
[12] Hutchins N, Marusic I. Evidence of very long meandering features in the logarithmic region of turbulent boundary layers. J Fluid Mech. 2007;579:1.
[13] Marusic I, Mathis R, Hutchins N. High Reynolds number effects in wall turbulence. Int J Heat Fluid Flow. 2010;31:418–428.
[14] Bandyopadhyay PR, Hussain AKMF. The coupling between scales in shear flows. Phys Fluids. 1984;27:2221–2228.
[15] Brown GL, Thomas ASW. Large structure in a turbulent boundary layer. Phys Fluids. 1977;20:S243–S252.
[16] Hutchins N, Marusic I. Large-scale influences in near-wall turbulence. Phil Trans R Soc Lond A. 2007;365:647–664.
[17] Marusic I, Mathis R, Hutchins N. Predictive model for wall-bounded turbulent flow. Science. 2010;329:193–196.
[18] Mathis R, Hutchins N, Marusic I. A predictive inner–outer model for streamwise turbulence statistics in wall-bounded flows. J Fluid Mech. 2011;681:537–566.
[19] Baars WJ, Hutchins N, Marusic I. Spectral stochastic estimation of high-Reynolds-number wall-bounded turbulence for a refined inner–outer interaction model. Phys Rev Fluids. 2016 (In Press).

[20] Mathis R, Marusic I, Chernyshenko SI, et al. Estimating wall-shear-stress fluctuations given an outer region input. J Fluid Mech. 2013;715:163.
[21] Grass AJ. Structural features of turbulent flow over smooth and rough boundaries. J Fluid Mech. 1971;50:233–255.
[22] Schultz MP, Flack KA. The rough-wall turbulent boundary layer from the hydraulically smooth to the fully rough regime. J Fluid Mech. 2007;580:381–405.
[23] Squire DT, Morrill-Winter C, Hutchins N, et al. Smooth and rough wall boundary layer structure from high spatial range particle image velocimetry. Phys Rev Fluids. 2016 (In Press).
[24] Baars WJ, Squire DT, Talluru KM, et al. Wall-drag measurements of smooth- and rough-wall turbulent boundary layers using a floating element. Exp Fluids. 2016;57:1–16.
[25] Nikuradse J. Laws of flow in rough pipes. 1933. (NASA Technical memorandum 1292).
[26] Ligrani PM, Moffat RJ. Structure of transitionally rough and fully rough turbulent boundary layers. J Fluid Mech. 1986;162:69–98.
[27] Castro IP, Segalini A, Alfredsson PH. Outer-layer turbulence intensities in smooth- and rough-wall boundary layers. J Fluid Mech. 2013;727:119–131.
[28] Morrill-Winter C, Squire DT, Klewicki JC, et al. Turbulent stress behaviours in boundary layers over sandpaper roughness. 2016 (In Preparation).
[29] Talluru KM, Baidya R, Hutchins N, et al. Amplitude modulation of all three velocity components in turbulent boundary layers. J Fluid Mech. 2014;746:R1.
[30] Chauhan KA, Monkewitz PA, Nagib HM. Criteria for assessing experiments in zero pressure gradient boundary layers. Fluid Dynam Res. 2009;41:021404.
[31] Sillero JA, Jiménez J, Moser RD. One-point statistics for turbulent wall-bounded flows at Reynolds numbers up to $\delta + \approx 2000$. Phys Fluids. 2013;25:105102.
[32] Smits AJ, McKeon BJ, Marusic I. High-Reynolds number wall turbulence. Ann Rev Fluid Mech. 2011;43:353–375.
[33] del Álamo JC, Jiménez J. Spectra of the very large anisotropic scales in turbulent channels. Phys Fluids. 2003;15:L41.
[34] Hutchins N, Nickels TB, Marusic I, et al. Hot-wire spatial resolution issues in wall-bounded turbulence. J Fluid Mech. 2009;635:103.
[35] Schultz MP, Bendick JA, Holm ER, et al. Economic impact of biofouling on a naval surface ship. Biofouling. 2011;27:87–98.
[36] Mathis R, Hutchins N, Marusic I. Large-scale amplitude modulation of the small-scale structures in turbulent boundary layers. J Fluid Mech. 2009;628:311.
[37] Taylor GI. The spectrum of turbulence. Proc R Soc Lond. A. 1938;164:476–490.
[38] Squire DT, Morrill-Winter C, Hutchins N, et al. Applicability of Taylor's hypothesis in rough- and smooth-wall boundary layers. J Fluid Mech. 2016 (Under Review).
[39] Marusic I, Monty JP, Hultmark M, et al. On the logarithmic region in wall turbulence. J Fluid Mech. 2013;716:R3.
[40] Monty JP, Chong MS, Mathis R, et al. A high Reynolds number turbulent boundary layer with regular 'Braille-type' roughness. In: IUTAM symposium on the Physics of wall-bounded turbulent flows on rough walls. Netherlands: Springer; 2010. p. 69–75.
[41] Anderson W. Amplitude modulation of streamwise velocity fluctuations in the roughness sublayer: evidence from large-eddy simulations. J Fluid Mech. 2016;789:567–588.
[42] Hutchins N. Large-scale structures in high Reynolds number wall-bounded turbulence. In: Progress in turbulence V. Switzerland: Springer International Publishing; 2014. p. 75–83.
[43] Townsend AA. The structure of turbulent shear flow. Vol. 2. Cambridge (UK): Cambridge University Press; 1976.
[44] Zhang C, Chernyshenko SI. Quasisteady quasihomogeneous description of the scale interactions in near-wall turbulence. Phys Rev Fluids. 2016;1:014401.
[45] Castro IP. Rough-wall boundary layers: mean flow universality. J Fluid Mech. 2007;585:469–485.